

Development of A Novel Dual-Layer Thick Ag Substrate for Surface-Enhanced Raman Scattering (SERS) of Self-Assembled Monolayers

Chad L. Leverette,[†] Virgil A. Shubert, Travis L. Wade, Kris Varazo, and Richard A. Dluhy*

University of Georgia, Department of Chemistry, Athens, Georgia 30602-2556

Received: February 18, 2002; In Final Form: May 21, 2002

A dual-layer, thick (~ 70 nm) vapor-deposited Ag substrate has been developed that gives enhancement factors on the order of 10^4 for surface-enhanced Raman scattering (SERS) experiments. This substrate has a total thickness of ~ 70 nm but also has an outermost surface morphology that approximates that of a thin Ag island film (AgIF) substrate. This is accomplished using a dual overlayer/underlayer structure in which a thick underlayer of 45-nm Ag is vapor-deposited onto a treated glass slide. This Ag underlayer is exposed to ambient conditions under which the surface chemisorbs oxygen, leading to the thermodynamically favorable formation of an active Ag_2O interface. An overlayer of 25-nm Ag is vapor-deposited on top of this structure. The first Ag/ Ag_2O underlayer produces an active interface that decreases the diffusion of the Ag atoms from the second vapor-deposited overlayer, thereby forming Ag particles with shapes favorable for SERS enhancement. Atomic force microscopy results show that the Ag overlayer particles have ideal shapes for SERS enhancement with morphology comparable to thin, vapor-deposited AgIFs. X-ray photoelectron spectroscopy in the O(1s) region showed the presence of multiple forms of oxygen in the Ag/ Ag_2O underlayer; the main forms were identified as dissolved bulk oxygen and chemisorbed oxygen. Using self-assembled monolayers (SAMs) of 1-dodecanethiol, a SERS intensity increase of $\sim 400\%$ was obtained for this new overlayer/underlayer Ag substrate when compared to SAMs formed on traditional thick Ag substrates. Enhancement factors calculated from the Raman intensity of *trans*-1,2-bis(4-pyridyl)ethane showed a SERS enhancement of approximately 10^4 for this new Ag/ Ag_2O /Ag substrate compared with the bulk. This compares favorably with the SERS enhancements obtained using thin AgIF substrates. The Ag/ Ag_2O /Ag substrates showed reproducible SERS intensities (RSD = 0.45–5%). The mechanisms responsible for the overall enhancement on this new substrate are proposed to be the ideal surface morphology of the Ag overlayer particles as well as a combined enhanced electromagnetic field produced by both the Ag/ Ag_2O underlayer and the Ag overlayer.

Introduction

Surface-enhanced Raman scattering (SERS) has emerged as a routine and powerful tool for the investigation and structural characterization of interfaces and thin-film solid materials. The excellent sensitivity and selectivity of SERS allows for the determination of chemical information from single monolayers on planar surfaces and extends the possibilities of surface vibrational spectroscopy to solve a wide array of chemical problems. Since the discovery of the SERS effect in the 1970s, this phenomenon has matured into a widely used technique.^{1–4} Comprehensive reviews on the SERS phenomenon have been published that discuss the fundamental mechanisms responsible for the effect as well as its applications.^{2,5–12} Despite its recent popularity, SERS does have its limitations, including strict requirements that must be met to achieve optimal enhancement. One of these requirements involves the critical need for an ideal surface morphology of the SERS metal substrate, a condition that is predicted from the long-range classical electromagnetic (EM) theory.^{9,13–15} Experimentally, the goal of achieving a reproducible surface morphology for a roughened metal surface can be quite challenging. This crucial limitation lends itself to the need for reproducible and practical SERS-active substrates.

As has been reviewed in detail elsewhere, two primary mechanisms are believed to be responsible for the SERS enhancement: a long-range^{16–22} classical electromagnetic (EM) effect and a short-range chemical (CHEM) effect.⁹ These two mechanisms contribute simultaneously to the overall enhancement in various amounts with the EM mechanism proposed to contribute the most ($\sim 10^4$) to the overall enhancement of the adsorbate while the CHEM mechanism is proposed to contribute a smaller amount ($\sim 10–10^2$).

The intensity enhancement attributed to the EM mechanism is due primarily to a localized surface plasmon resonance.¹⁵ The criteria for production of a surface plasmon depend on the excitation frequency and the dielectric constants of the surface. When excited with visible light, the free-electron metals (i.e., Ag, Au, Cu) fulfill the necessary surface plasmon requirements by having dielectric constants with a large negative real component and a small imaginary component.^{12,23} Therefore, these metals are the substrates of choice for SERS experiments. For Ag, the real component of its dielectric constant gives an optimized local electric field for small, spherical Ag particles with radii less than 25 nm when using visible excitation.¹² For this reason, Ag has become a popular SERS substrate.

In predicting the optimal SERS enhancement, the importance of the morphology of the metal particles on the substrate's surface cannot be underestimated. The particle shape and radius of curvature of each metal particle on the surface govern the

* To whom correspondence should be addressed. Office: 706-542-1950. Fax: 706-542-9454. E-mail: dluhy@chem.uga.edu.

[†] Current address: Cargill, Inc., Memphis Analytical Technology Center, 7101 Goodlett Farms Parkway, Cordova, TN 38016.

relationship between scattering intensity and the distance of the adsorbate from the surface, as well as the overall enhancement.²⁴ EM theory predicts that a range of Ag particle sizes (from rough Ag particles with radii less than 25 nm down to clusters of four Ag atoms) can potentially be used to achieve high SERS enhancement,^{12,25,26} although a limitation to EM theory is that these calculations take into consideration only a single metal particle with ideal shape. EM theory does not consider particle–particle interactions, adsorbate–adsorbate interactions, or inhomogeneous particle size and shape distributions on the metal surface, conditions that exist on all SERS substrates and that contribute to SERS efficiency.

Many substrate preparation techniques exist that attempt to form metal surfaces consisting of an ideal SERS surface morphology. The discovery of the SERS effect occurred on a Ag electrode that became SERS-active upon the roughening of the surface by oxidation–reduction cycles (ORC).¹ Consequently, this is a popular method of substrate preparation and achieves the highest SERS enhancement factors, although it is a difficult method to reproduce and results in the production of substrates with nonuniform, pitted surfaces. A widely used nonelectrochemical method of SERS substrate preparation is the use of metal sols, which are prepared by chemically reducing a dilute solution of a metal salt. However, the experimental variables for producing colloidal dispersions are difficult to control and this method is plagued by the aggregation of the colloids into macroscopic particles. Other methods that attempt to fabricate an ideal Ag surface morphology for SERS substrates include laser ablation of metals by high-power laser pulses,²⁷ acid-etched Ag foils, roughened films prepared by Tollen's reagent, and photodeposited Ag films on anatase TiO₂.²⁸

Of all the methods discussed above, none have the potential for reproducibility and stability like vapor-deposited Ag metal films.²⁴ The vapor deposition method results in a film of discontinuous particles of ellipsoidal geometry. These silver island films (AgIF) are more stable than metal sols and produce a surface of particles that are more uniform in shape than the electrochemical method. To obtain the optimal shape for the Ag particles, the experimental variables of vapor deposition must be controlled, which include proper substrate material, temperature of the substrate during and following the deposition, total thickness of the film, and rate of deposition.²⁴ Control of these variables results in surfaces of reproducible roughness features across a given metal film. Vapor-deposited substrates have the potential to selectively “tune” the electromagnetic properties of a surface for a given experiment.²⁹ SERS EM theory predicts relatively small enhancements (~4–30) for smooth metal surfaces;¹⁴ therefore, the total thickness for SERS-active vapor-deposited films has been kept to less than 10 nm. This thickness limitation helps to maintain the ideal rough surface morphology of ellipsoidal metal clusters.

While thin, vapor-deposited Ag films have been successfully employed as SERS substrates, a thick metal film would be advantageous in Raman experiments for several reasons. (1) A thick film would allow the excitation radiation to avoid striking the underlying substrate, which generates unwanted background in the spectrum (i.e., substrates are commonly glass slides, which have a characteristic Raman spectrum). (2) Thick films have minimal specular reflectance from the reflecting laser beam compared to traditional thin metal films. (3) The same metal film could be used for a dual experiment utilizing SERS and Infrared Reflection–Absorption Spectroscopy (IRRAS) to gain a complete vibrational characterization of a given adsorbate. Thick (>10 nm) metal films have not been frequently used as

SERS substrates. Two papers have appeared that use these types of substrates; one dealt with the use of cold-deposited thick Ag films³⁰ and the other discussed SERS-active thick films vapor-deposited on top of polymer nanospheres.²⁹

In this paper, we describe the preparation of a thick Ag SERS substrate that has a total thickness of ~70 nm but also has an outermost surface morphology that approximates that of an ideal thin AgIF. This is accomplished using a dual overlayer/underlayer structure consisting of two distinct vapor-deposited layers of Ag clusters separated by an active Ag₂O oxide layer formed by chemisorption of ambient O₂ that adheres to the first Ag underlayer. We have characterized the formation of this novel substrate using atomic force microscopy and X-ray photoelectron spectroscopy. Using this substrate, we studied the SERS spectra of self-assembled monolayers (SAMs) of 1-dodecanethiol. An intensity increase of ~400% was obtained for this novel overlayer/underlayer Ag substrate compared to SAMs formed on traditional thick Ag substrates. Enhancement factors were calculated from observation of the Raman signal intensity from adsorbed molecules of *trans*-1,2-bis(4-pyridyl)ethene and are about 10⁴ for this new substrate. Analysis of multiple samples showed that the SERS intensity from SAMs adsorbed onto these new substrates is reproducible to within ±5%.

Materials and Methods

Reagents. Water was filtered and deionized using a Barnstead Nanopure reverse osmosis/deionization system to a resistance of 18.2 MΩ. A Piranha solution consisting of 1:4 30% H₂O₂/ACS reagent grade concentrated H₂SO₄ (J. T. Baker) was used to clean all glassware. (3-Mercaptopropyl)trimethoxysilane (97%) (MPS) (Alfa Aesar, Ward Hill, MA) and HPLC grade 2-propanol (J. T. Baker) were used for the pretreatment of the substrate. Silver wire (100% purity) was obtained from SPI (West Chester, PA). 1-Dodecanethiol (98%) (Aldrich) and 200 proof ethanol (Pharmco, Brookfield, CT) were used for the self-assembly of molecular monolayers. A 2.0 × 10⁻⁴ M solution of *trans*-1,2-bis(4-pyridyl)ethene (Aldrich) in HPLC grade methanol (J. T. Baker) was used to calculate the enhancement factors. All reagents were used as received.

Substrate Preparation. Glass microscope slides (VWR Scientific; 25 mm × 75 mm) were used as the substrate. The slides were cut to dimensions of 1.5 cm × 1.5 cm. Visible residue was wiped off of the surfaces of the cut slides which were then immersed into a 1:4 H₂O₂/H₂SO₄ (Piranha) solution at >70 °C for about 15 min. The slides were then rinsed with H₂O, stripped of visible surface water with a stream of N₂, and placed in an oven at ~110 °C for 10 min. MPS application followed published procedures.³¹ MPS was applied from a boiling aqueous alcohol solution. The silanization solution consisted of 10 g MPS in 10 g H₂O + 400 g of 2-propanol. This solution was brought to a boil, and the clean, dry, cut slides were immersed into this solution for 10 min. After 10 min, the slides were carefully rinsed with 2-propanol and blown dry with a gentle stream of N₂. The slides were then placed into a drying oven (~110 °C) to cure. This MPS application procedure was carried out twice.

Formation of Vapor-Deposited Silver Island Films (AgIF). Silver vapor deposition was carried out in a conventional vacuum deposition bell jar system equipped with a resistive heating evaporation apparatus. The clean, MPS treated slides were placed ~10 cm above a tungsten boat (SPI, West Chester, PA) containing silver wire. The chamber was evacuated to a pressure <1 × 10⁻⁶ Torr for silver deposition. A current of approximately 8.0 A vaporized the Ag. The typical deposition rate was ~0.5 nm/sec (estimated).

The total thickness of each film was monitored by ellipsometry. Ellipsometric measurements were performed using a multiangle Sentech SE 400 ellipsometer (Micro Photonics Inc., Allentown, PA). Each thickness measurement was the average of at least three different spots per film and was reproducible in thickness to within ± 1 nm. The reproducibility for consecutive films of the same thickness also varied within 2-nm total thickness (RSD is less than $\pm 3\%$). The average total thickness was divided by the total time of the evaporation to estimate a deposition time. The reproducibility of this method was proven through SERS activities and AFM measurements of each film.

Self-Assembly of 1-Dodecanethiol. The AgIF surfaces were immersed in a 15 mM 1-dodecanethiol solution in 100% ethanol for at least 12 h to allow the self-assembled monolayers to form. These surfaces were then removed from the solution, rinsed carefully with copious amounts of 100% ethanol, and allowed to completely air-dry before analysis took place.

Atomic Force Microscopy Measurements. The AgIF surfaces were profiled using a Nanoscope III (Digital Instruments, Santa Barbara, CA) atomic force microscope. The images described in this article were obtained using constant-force mode, where the piezo moved the sample to keep the cantilever deflection signal essentially constant. The cantilevers were 115 μm in length with Si_3N_4 tips, and the backsides were coated with Au to reflect the laser beam used to monitor the deflection. The spring constant of the tips was 0.58 N/m. All images presented in this article represent raw data obtained in air. Topographical roughness profiles were extracted from digital image data using a postacquisition line section analysis program.

X-ray Photoelectron Spectroscopy (XPS). XPS spectra were collected using an unmonochromatized X-ray source (VG Scientific) and hemispherical analyzer (Leybold–Heraeus) mounted in an ultrahigh vacuum chamber (UHV) with a base pressure of 1×10^{-9} Torr, maintained with an ion pump and cryopump. The sample was placed into the chamber by introduction into an antechamber under an atmosphere of high purity argon (BOC). After pumping away the argon and reaching UHV pressures, the sample was transferred into the main chamber for analysis. XPS spectra were obtained using Al $K\alpha$ X-rays (1486.6 eV). The gold $4f_{7/2}$ peak (83.98 eV) was used for calibration.³²

Surface-Enhanced Raman Scattering. The Raman instrument used in these experiments consisted of an ISA 500M $f/4$ monochromator equipped with a Spectrum One CCD2000 charge-couple device detector (Instruments SA, Edison, NJ). The CCD chip (SiTe ST-005A) was 2000×800 pixels in size, back-illuminated, with an individual pixel size of $15 \mu\text{m}$. The detector was LN_2 -cooled to a temperature of -140 °C and back-thinned, resulting in a QE of 85% at 550 nm. The grating used in the spectrometer had 1200 grooves/mm with a blaze wavelength of 750 nm. The slit widths used in the experiments were typically 0.30 mm.

The optical interface used for the collection of the surface-enhanced Raman spectra has been described in detail elsewhere.³³ The excitation was incident on the sample at an angle of 60° and was produced by the 514.5-nm line of a Coherent Radiation Innova 300 Series Ar⁺ laser. The typical laser power at the sample was 150 mW with an average spot size of $30 \mu\text{m}$ in diameter. The scattered radiation was collected at the surface normal through an optical interface designed in our lab.³³ Integration times were typically 60 s with 5 coadds. For the *trans*-1,2-bis(4-pyridyl)ethene (BPE) experiments, a single spectrum was collected using a 5 s integration time. Baseline correction and spectral averaging were accomplished using the

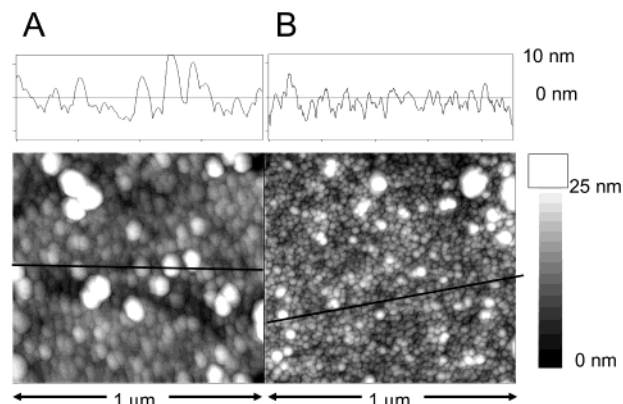


Figure 1. (A) A representative AFM image with corresponding line scan plot of the traditional thick Ag island film (AgIF) substrate (45-nm thick). (B) A representative AFM image with corresponding line scan plot from the AFM image of the overlayer/underlayer Ag substrate (total 70-nm thick). Ag substrates were prepared at room temperature with a deposition rate ~ 0.5 nm s^{-1} .

GRAMS/32 (Galactic Industries, Salem, NH) software package. CCD spike removal was accomplished using a statistical approach for identification of spurious signals;³⁴ this algorithm was adapted in our laboratory for the Grams/32 environment. The SERS spectra presented here have not been smoothed.

Results and Discussion

Characterization of Ag Overlayer/Underlayer Substrates by Atomic Force Microscopy. We have constructed a thick Ag substrate consisting of an overlayer/underlayer structure vapor-deposited onto glass. The initial step in creation of this substrate involved producing the underlayer structure by vapor depositing a Ag layer of ~ 45 -nm thickness onto MPS-treated glass slides. Once this initial Ag deposition was complete, the film was removed from vacuum and allowed to sit under ambient conditions for at least 12 h. After this time period, the film was placed back into the bell jar system and a second layer of Ag (25-nm thick) was deposited onto the first layer to create the overlayer. Both depositions followed the experimental conditions described in the Materials and Methods section. After the overlayer was complete, the film was removed from vacuum and immediately used for the self-assembly of alkanethiol monolayers.

The substrates created by this dual-step vapor deposition process were characterized using atomic force microscopy. AFM has been shown to be a powerful tool in determining morphological properties of Ag island films (AgIF). In particular, a correlation has been demonstrated between the Ag island particle shape and the requirements for optimal SERS enhancement as predicted by EM theory.²⁹ A parameter called the shape factor, $R = b/a$, was introduced, which is defined as the ratio of the semiminor axis (particle height = b) to the semimajor axis (particle diameter = a). The shape factor identifies a given particle as prolate ($R > 1$), oblate ($R < 1$), or spherical ($R = 1$). The larger the departure from a spherical shape, the stronger the local electric field (E_L) will be and hence the more SERS active the particle.¹⁵ The shape factor, R , successfully relates the optical properties (i.e., plasmon resonance frequency) of thin, vapor-deposited AgIF substrates to their SERS activities. The optimum Ag thickness providing the greatest SERS enhancement was shown to be 8 nm because of the oblate nature ($R = 0.36$) of the Ag particles.²⁹

We have analyzed the nature of the new dual overlayer/underlayer Ag substrate using AFM. Figure 1A shows a

TABLE 1: Particle Size and Shape Properties for a Thick (45-nm) Ag Substrate and for an Overlayer/Underlayer Substrate (Ag/Ag₂O/Ag, 25-nm Overlayer/45-nm Underlayer; 70-nm Total Thickness)^a

substrate thickness (nm)	particle size (nm)		
	a	b	$R = b/a$
45	68.9 ± 21.3	7.9 ± 5.2	0.11 ± 0.04
70	31.5 ± 6.7	6.7 ± 1.9	0.21 ± 0.03

^a Particle sizes values are reported as mean \pm RSD for 30 individual Ag particles obtained from AFM images.

representative AFM image of a traditional thick Ag vapor-deposited film (45-nm total thickness), while Figure 1B shows a substrate prepared by our dual overlayer/underlayer Ag deposition technique (70-nm total thickness). It is clear from these images that the particles in the image of the dual overlayer/underlayer Ag substrate are smaller, more uniform, and more isolated than the traditional thick surface.

Line section analysis was performed on these images to gain further insight into the topography of these substrates. Figure 1A shows line section analysis data for a traditional 45-nm thick Ag substrate. The surface in Figure 1A is very nonuniform with particles that are fairly large in diameter because of the coalescence of individual particles. The spaces between the particles create smooth valleys of small overlapped particles with no distinguishable shape. This is a typical morphological representation of a thick metal substrate. In contrast, Figure 1B shows the line section analysis for a substrate prepared using the overlayer/underlayer Ag technique with a total thickness of 70 nm. The line section illustrates that the Ag particles in this new substrate are indeed smaller, more separated, and hence create a more uniform surface. While the dual-layer substrate illustrated in Figure 1B does contain some large coalesced particles such as the thick surface, the number of these particles is much smaller than in the traditional thick surface.

The shape factor R was calculated for both of these substrates in a manner similar to that previously described,²⁹ and the data is reported in Table 1. The determination of the shape factor helps to quantify the images in Figure 1. The particle diameters and heights reported in Table 1 were determined from the line section graphs of each substrate; these numbers are the mean \pm standard deviation for 30 particles in the field of view. To ensure a representative sampling, at least three random line sections were obtained to allow the selection of a minimum of 30 particles. Therefore, the R values in Table 1 are also presented as mean \pm standard deviation for a minimum of 30 particles.

For the traditional thick Ag substrate, our value for $R = 0.1$ is consistent with the shape factor previously calculated for a relatively thick 16-nm film that exhibited reduced SERS enhancement.²⁹ This observation agrees with the proposed theory that as the surface becomes thick (> 10 nm) the Ag particles exhibit increased particle–particle interactions; the coalescence of the particles causes an increase in grain size and hence a smoothing of the surface.³⁸ A smooth, thick surface will be comprised of these large, oblate, layered particles that are not optimal for SERS enhancement.

An R value of 0.21 was calculated for the 70-nm overlayer/underlayer substrate (Table 1). The particle diameters and heights of the new overlayer/underlayer substrate agree with previously published data for particles in an 8-nm thin AgIF substrate that showed maximum SERS enhancement. The calculated shape factor for the new overlayer/underlayer Ag substrate ($R = 0.21$), however, is somewhat smaller than the one previously calculated ($R = 0.36$) for the 8-nm thin Ag film that exhibited the best SERS enhancement.²⁹ Although the R

values differ slightly, a comparison of our current results with the previous study of thin AgIFs for SERS substrates produces some striking similarities. In particular, particles for the new overlayer/underlayer Ag substrate are oblate and well separated, leading to a surface that has an optimal shape for SERS enhancement. The AFM data indicate that the new thick (70-nm) overlayer/underlayer Ag substrate described here has a similar outermost surface morphology to that of a traditional thin (< 10 -nm) AgIF substrate that exhibited maximal SERS enhancement.

Formation of 1-Dodecanethiol Self-Assembled Monolayer Films. Self-assembled monolayers have received a great deal of attention in the literature because of their use in applications ranging from biosensors and protective layers to surface and electrode modification.³⁵ 1-Dodecanethiol adsorbed to a roughened silver surface has been widely used as a model system.^{22,23} This alkanethiol SAM has been studied and characterized using SERS.²⁵ Therefore, for comparison with this previous work in the literature, self-assembled monolayers of 1-dodecanethiol were selected as the model system to study using the new overlayer/underlayer Ag substrate.

Figure 2 shows representative SERS spectra of 1-dodecanethiol SAMs adsorbed onto two different Ag substrates: a traditional 45-nm thick Ag substrate and a thick Ag substrate produced from our overlayer/underlayer deposition method. Figure 2A.a shows the $\nu(\text{C}-\text{H})$ stretching region in the SERS spectrum of 1-dodecanethiol on a 45-nm thick AgIF. The S/N for the symmetric methylene stretch, $\nu_s(\text{CH}_2)$ in Figure 1A (a) at $\sim 2852 \text{ cm}^{-1}$ is ~ 122 . Figure 2A.b is also the SERS spectrum of 1-dodecanethiol but adsorbed onto the roughened silver surface produced by the new overlayer/underlayer vapor deposition process. The S/N ratio for the $\nu_s(\text{CH}_2)$ at $\sim 2852 \text{ cm}^{-1}$ on this surface is ~ 420 . Figure 2B presents the same SERS spectra as in Figure 2A but in the low wavenumber region centered on the $\nu(\text{C}-\text{C})$ stretching bands at 1100 cm^{-1} . Figure 2B.a illustrates the SERS spectrum for a 1-dodecanethiol SAM in this region for the 45-nm thick AgIF, while Figure 2B.b is the same SAM but adsorbed on the new overlayer/underlayer AgIF substrate. A comparison of the intensities of the two SERS spectra of 1-dodecanethiol in these two spectral regions demonstrates a SERS intensity increase of at least 400% for 1-dodecanethiol SAMs on the new overlayer/underlayer Ag substrate compared to a traditional thick Ag substrate.

The structure and orientation of 1-dodecanethiol SAMs have been studied using SERS on roughened Ag surfaces.²⁵ Because of the shorter chain length, SAMs of 1-dodecanethiol possess a higher degree of gauche conformers as compared to the SAMs of the other longer chain alkanethiols. The proposed orientation of 1-dodecanethiol allows the C–S bond and the C–C backbone to be mostly perpendicular to the surface with the plane of the carbon backbone tilted $\sim 15^\circ$. The wavenumber position and intensity of the vibrational bands of the 1-dodecanethiol SAMs presented in Figure 2A.b and Figure 2B.b agree with the previous SERS results.²⁵ Therefore, the molecular structure and orientation for 1-dodecanethiol SAMs adsorbed on the new overlayer/underlayer Ag substrate are likely to be similar to 1-dodecanethiol SAMs formed on thin AgIF substrates.

Optimal Ag Overlayer/Underlayer Thickness/Calculation of Enhancement Factors (EF). In developing the new overlayer/underlayer Ag substrate, we have examined the optimum thickness for both underlayer and overlayer that lead to the maximum SERS enhancements. In one such study, we analyzed the variation in SERS enhancement as a function of thickness for a traditional thick Ag substrate. In this experiment, 1-dode-

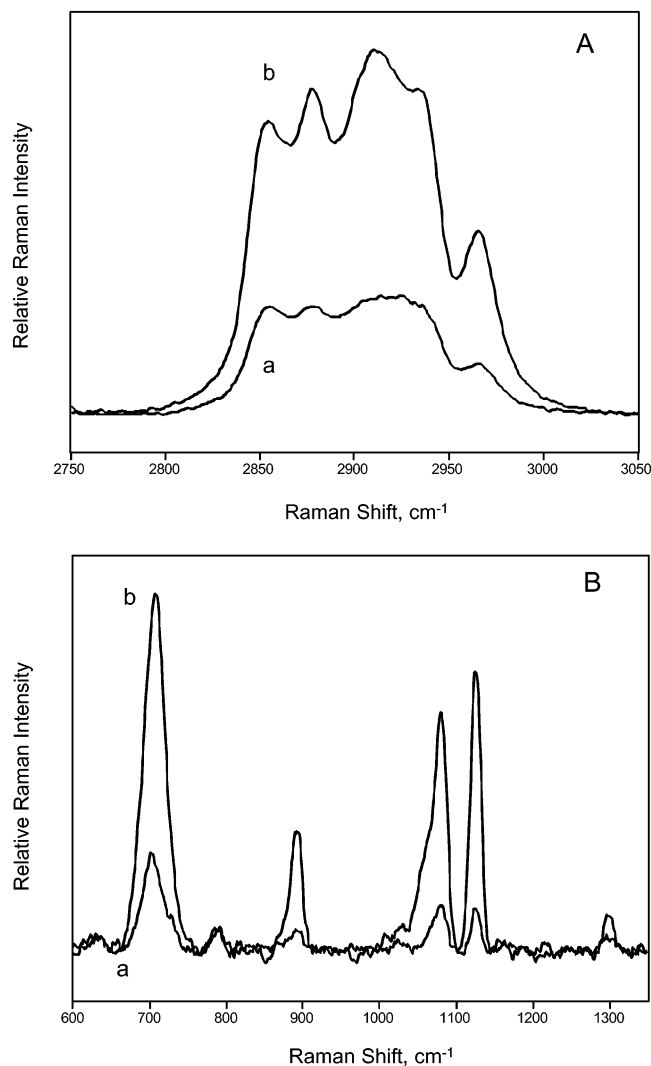


Figure 2. (A) SERS spectrum in the $\nu(\text{C-H})$ stretching region for a 1-dodecanethiol SAM adsorbed (a) onto a traditional thick Ag substrate (45-nm thick) or (b) onto the overlayer/underlayer Ag substrate (total 70-nm thick). (B) SERS spectrum in the $\nu(\text{C-C})$ stretching region for a 1-dodecanethiol SAM adsorbed (a) onto a traditional thick Ag film (45-nm thick) or (b) onto the overlayer/underlayer Ag substrate (total 70-nm thick).

canethiol SAMs were adsorbed onto thick vapor-deposited Ag substrates and the variations in SERS activities for the C-H band at 2852 cm^{-1} were monitored. This particular vibration was chosen for comparison among different samples since its intensity is not affected by changes in orientation like the $\nu(\text{C-S})$, $\nu(\text{C-C})$, or the $\nu(\text{CH}_3)$ methyl group bands.²⁵ Therefore, this vibrational mode will not change intensity for slight reordering within the SAM but rather will be a reliable indicator of the SERS enhancement of the underlying substrate.

Figure 3 demonstrates that no real pattern for SERS enhancement is observed for a traditional thick Ag substrate as the Ag thickness increases. Upon repeated experiments, we observed that a 45-nm thick film gave, on the average, the strongest SERS enhancements of the thick Ag substrates studied. As discussed above, none of these substrates are expected to demonstrate strong SERS enhancement because of the morphology of their surface Ag particles. AFM showed that these thick Ag substrates are comprised of a vast array of large, oblate particles that have overlapped and coalesced (see, e.g., Figure 1A).

In the studies reported in this section, we endeavored to create reproducible procedures for monitoring SERS enhancements

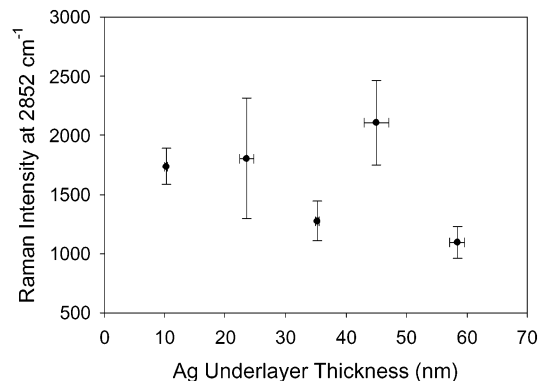


Figure 3. Intensity variation of the SERS 2852 cm^{-1} symmetric methylene vibrational band, $\nu_s(\text{CH}_2)$, from 1-dodecanethiol SAMs as a function of the increasing thickness of a traditional thick Ag substrate. Y-axis error bars report the mean \pm RSD for the SERS band intensity. X-axis error bars reflect the mean \pm RSD for the overall thickness of each film as analyzed by ellipsometry.

among different samples. To do this, we monitored the band height from the center-of-gravity calculated peak position to the zero baseline for the 2852 cm^{-1} vibration. Three different samples of the same thickness with three different spots per sample were analyzed by SERS. The mean and standard deviations of the observed SERS intensity for each Ag thickness were calculated and reported as error bars along the y (Raman intensity) axis in Figure 3. The thickness of each Ag substrate was measured by ellipsometry. For the x (Ag substrate thickness) axis in Figure 3, the error bars demonstrate the vapor deposition procedure (as monitored by ellipsometry) produces highly reproducible, thick Ag substrates (RSD for substrate thickness less than $\pm 3.5\%$). In contrast to the reproducibility of the Ag thickness, Figure 3 shows that the SERS intensities measured from the 2852 cm^{-1} band of 1-dodecanethiol SAMs are not highly reproducible for a thick Ag substrate. The relative standard deviations for the SERS intensity varied from $\pm 12\%$ for a 10-nm thick Ag substrate to $\pm 28\%$ for the 24-nm thick Ag substrate and $\pm 17\%$ for the 45-nm Ag substrate.

To determine the Ag overlayer thickness that provides a maximal SERS enhancement for the overlayer/underlayer substrate, samples having a thick underlayer of 45-nm Ag were prepared and allowed to oxidize in ambient conditions for 12 h. These surfaces were then placed back into the vacuum apparatus and samples were prepared with vapor-deposited Ag overlayers of varying thickness. SAMs of 1-dodecanethiol were formed on the resulting overlayer/underlayer Ag substrates and the SERS intensities were determined for these samples. Figure 4 shows the results of this study. In contrast to Figure 3, a definite pattern is shown for the SERS intensity of the 2852 cm^{-1} band as a function of overlayer thickness. The optimal intensity is for an overlayer with thickness equal to 24 nm with an RSD of less than 5%, while overlayer thickness either greater or less than 24 nm produced decreased SERS intensity. The thinnest overlayer studied (10 nm) not only had reduced SERS intensities but also had the largest RSD for the measured intensities at $\sim 20\%$.

A possible explanation for the pattern of SERS intensities observed in Figure 4 involves the "filling in" of the nonuniform features of the 45-nm Ag underlayer. A 10-nm Ag underlayer is too thin to cover all the nonuniform morphological features of the underlayer; therefore, the underlayer morphology still primarily influences the SERS intensity for this substrate. At an overlayer thickness of 24 nm, however, the underlayer texture is sufficiently covered by overlayer Ag so that it is the overlayer

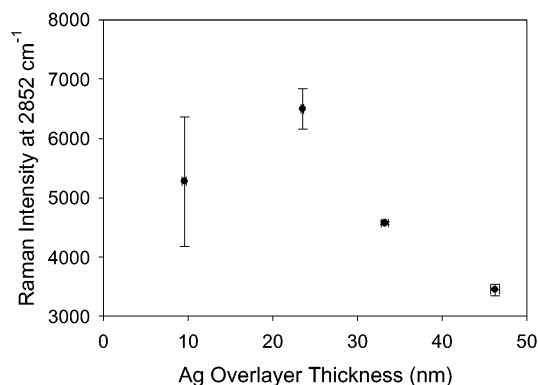


Figure 4. Intensity variation of the SERS 2852 cm⁻¹ symmetric methylene vibrational band, $\nu_s(\text{CH}_2)$, from 1-dodecanethiol SAMs adsorbed onto Ag overlayers of increasing thickness on top of a constant thickness (45-nm) Ag underlayer. Y-axis error bars report the mean \pm RSD for the SERS band intensity. X-axis error bars reflect the mean \pm RSD for the overall thickness of each film as analyzed by ellipsometry.

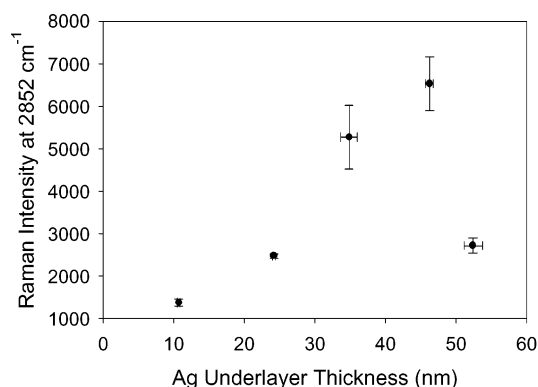


Figure 5. Intensity variation of the SERS 2852 cm⁻¹ symmetric methylene vibrational band, $\nu_s(\text{CH}_2)$, from 1-dodecanethiol SAMs adsorbed onto a constant thickness (24-nm) Ag overlayer as the Ag underlayer thickness was varied. Y-axis error bars report the mean \pm RSD for the SERS band intensity. X-axis error bars reflect the mean \pm RSD for the overall thickness of each film as analyzed by ellipsometry.

structure that controls SERS intensity. In addition, the 24-nm overlayer Ag particles are likely hindered from diffusion because of the underlayer morphology and the presence of interlayer Ag₂O (described in more detail in the next section). This leads to a surface that has a more ideal shape for SERS activity. For thicker overlayers, the intensity drops because the number of atoms coming to the surface increases and allows the overlayer to coalesce and take on the appearance of a traditional thick Ag substrate.

We have confirmed that the optimal Ag thickness for the overlayer/underlayer substrate is approximately 45 nm/24 nm by holding the Ag overlayer thickness constant at 24 nm while varying the thickness of the Ag underlayer substrate (Figure 5). These data clearly indicate a definite dependence of the SERS intensity for the overlayer/underlayer substrate on the Ag underlayer thickness. There is a remarkable sensitivity to the thickness dependence of the underlayer. Although increasing the thickness of the Ag underlayer from 10 to 45 nm results in an increase of $\sim 400\%$ in overall SERS intensity for the combined overlayer/underlayer substrate, a further increase in the thickness from 45 to 50 nm results in a dramatic decrease of $\sim 60\%$ in the observed SERS intensity.

The molecular probe *trans*-1,2-bis(4-pyridyl)ethene (BPE) was used to calculate the SERS enhancement factor (EF) for

the traditional thick Ag film as well as the overlayer/underlayer Ag substrate. BPE was chosen for its high Raman scattering cross section, its nonresonant enhancement in the visible region, and its ability to bind efficiently to a Ag surface. The EF is defined as the ratio of the adsorbate's SERS intensity to its bulk, normal Raman intensity, that is, $I(\nu)_{\text{surface}}/I(\nu)_{\text{bulk}}$. Each of these intensities has been normalized for the effects of surface versus volume number density for the molecules observed. For this experiment, the laser power and the integration time remained constant for both bulk and surface analysis. We compared the SERS intensity of the 1200 cm⁻¹ band for this molecular probe because of this band's relative insensitivity to molecular orientation.²⁸ The combination of the surface coverage of BPE and the area probed by the laser excitation spot resulted in $\sim 3.01 \times 10^8$ BPE molecules analyzed on each Ag substrate. For the bulk solution experiments, the number density probed by the laser spot was $\sim 1.28 \times 10^{11}$ molecules. The SERS intensity of the 1200 cm⁻¹ band of BPE on the overlayer/underlayer Ag geometry was 2000 counts s⁻¹, on the traditional thick Ag substrate it was 100 counts s⁻¹, and for a 2.0×10^{-4} M bulk solution the Raman intensity was 75 counts s⁻¹. This leads to an EF of 1.13×10^4 for the new overlayer/underlayer Ag substrate at 514.5 nm compared with an EF of 5.67×10^2 for the BPE adsorbed onto the traditional thick Ag substrate. The value of 10^4 for the overlayer/underlayer Ag substrate agrees with the EFs previously calculated for adsorbates on thin, vapor-deposited AgIF substrates in the visible region.^{5,29}

Chemisorption of O₂ onto the Ag Underlayer. Our hypothesis for the increased SERS intensities observed using the overlayer/underlayer Ag substrate postulates an intermediate step involving the 45-nm vapor-deposited Ag underlayer. It is presumed that the thick Ag underlayer will immediately physisorb oxygen upon its removal from the vacuum deposition apparatus. If exposed to ambient conditions, the thick Ag substrate will become passivated by a monolayer of chemisorbed oxygen, forming a surface layer of Ag₂O. It is upon this Ag/Ag₂O underlayer that the second overlayer of Ag is deposited. Because of the morphology of the underlying thick Ag underlayer substrate and the presence of an active oxide interface, the Ag particles of the second layer will be trapped into smaller particle diameters by a decrease in their rate of diffusion and coalescence. These overlayer Ag particles can then form a surface morphology similar to that of a traditional thin AgIF that allows for enhanced SERS intensities. The AFM data presented in Figure 1B support this interpretation.

This interpretation is also supported by previous studies of the interaction of oxygen with Ag particles via chemisorption.³⁶ These studies concluded that Ag nanoparticles are chemically active on the surface and can interact with the oxygen in ambient air first by physisorption and then by chemisorption.

The role that O₂ adsorption plays in the formation of a SERS active Ag overlayer/underlayer substrate can be illustrated. An experiment was performed in which both Ag underlayer and overlayer were deposited as usual, but vacuum was never broken. Thus, the thick Ag underlayer was never exposed to ambient conditions. In this experiment, a 45-nm thick Ag substrate underlayer was vapor-deposited onto a glass slide and left in the vacuum deposition apparatus overnight. After 12 h, a 24-nm Ag overlayer was deposited onto the underlayer. After removal from the vacuum system, 1-dodecanethiol SAMs were prepared and SERS spectra of these monolayers were acquired. The intensities of the SERS bands for this nonoxidized overlayer/underlayer Ag substrate were weak (data not shown) and resembled the intensities obtained for a traditional thick

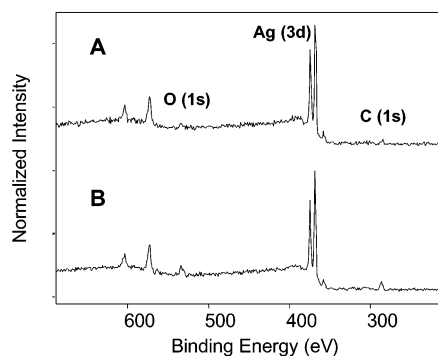


Figure 6. (A) XPS spectra of a thick 45-nm Ag substrate analyzed immediately after vapor deposition. (B) XPS data of a thick 45-nm Ag substrate analyzed after the substrate had remained in ambient conditions for approximately 12 h.

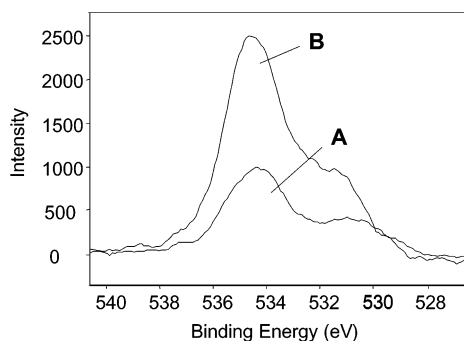


Figure 7. (A) XPS data in the O(1s) region of a thick 45-nm Ag substrate analyzed immediately after vapor deposition. (B) XPS data in the O(1s) region of a thick 45-nm Ag substrate analyzed after the substrate had remained in ambient conditions for approximately 12 h.

Ag substrate (see Figure 2A.a and Figure 2B.a). These results demonstrate that the presence of an oxidized Ag interface is necessary for the enhanced SERS intensities observed in the Ag/Ag₂O/Ag substrate.

Characterization of the Ag/Ag₂O Surface Using X-ray Photoelectron Spectroscopy. X-ray photoelectron spectroscopy (XPS) was used to identify the constituents that adsorbed to the underlayer surface after the substrate was removed from vacuum. Previous XPS studies have discussed the oxidation of Ag(111) under various conditions;^{37,38} the band positions we report are based on the assignments made in these studies. Our XPS spectra (Figures 6 and 7) compare well with reference spectra³² and show the presence of a clean Ag substrate with O₂ and C being the only contaminants present.

XPS spectra were obtained of two different 45-nm thick Ag substrates after vapor deposition. The first substrate was a Ag underlayer removed immediately from the vacuum apparatus and placed into the ultrahigh vacuum (UHV) apparatus for XPS analysis (Figure 6A). The other sample was a Ag underlayer that had been removed from vacuum and allowed to sit in the ambient environment for 12 h (Figure 6B). Figure 6 shows that both substrates are spectroscopically similar with the only difference being a slight increase in the intensity of the O₂ and C bands for the film left out in ambient conditions. We attribute the trace amounts of C in Figure 6A to carbon residue from the oil-based diffusion pump of the vapor depositor. The slight increase in the 272 eV C band in Figure 6B results from environmental contamination after exposure to ambient conditions.

The O(1s) region was analyzed to determine the different forms of oxygen present in the Ag underlayer. Figure 7 shows the O(1s) region in the XPS spectra of the two thick Ag substrates; this region appears as a broad doublet for both

samples. For the thick Ag underlayer substrate analyzed immediately upon removal from the vacuum deposition apparatus (Figure 7A), several XPS bands are seen. The main peak in this spectrum appears at ~534 eV and is assigned to oxygen in the bulk metal. A broad shoulder is seen at lower eV that likely consists of two additional bands, one at ~530.4 eV because of chemisorbed surface oxygen and a shoulder at ~531 eV because of residual oxygen contamination. This interpretation is made somewhat tentatively since we are using a rough substrate morphology compared to the Ag(111) single crystal used to collect the standard XPS spectra.^{37,38} Nonetheless, it is clear from Figure 7 that several forms of oxygen are present in the Ag underlayer substrate.

A slight increase in the intensity of the O(1s) region resulted in the Ag underlayer substrate that remained in ambient conditions for 12 h (Figure 7B). This spectrum indicates that the Ag substrate can undergo a slight further oxidation with time, even though the surface appears passivated by O₂ directly upon removal from the vacuum deposition apparatus (Figure 7A). The main difference in the XPS spectra of the two Ag underlayer substrates is in the ~534 eV band, which is associated with dissolved bulk oxygen. This is consistent with the diffusion of the metal clusters on the surface, in which physisorbed oxygen can rearrange and diffuse into the bulk metal with time.

Evidence for a Combined Enhanced Electric Field from the Underlayer (Ag/Ag₂O) and the Overlayer (Ag). As described above, the hypothesis for the increased SERS intensity observed using the overlayer/underlayer Ag/Ag₂O/Ag substrate postulates the presence of an intermediate Ag₂O layer between the Ag overlayer and Ag underlayer. As the XPS data demonstrates, the thick Ag underlayer substrate does become passivated by chemisorbed oxygen, forming a surface layer of Ag₂O.

We propose that the mechanism for the observed SERS enhancement includes a contribution from a combined electric field arising from both the Ag/Ag₂O underlayer as well as the Ag overlayer. This E-field enhancement mechanism is similar to that previously described for a sandwich-type SERS substrate in which the overlayer was deposited on top of the sample.³⁹ The combined electric field mechanism rests on two assumptions: (1) that the two layers are separated by a surface oxide layer and (2) that the difference in morphology between the surfaces is significant. The XPS data in the O(1s) region (Figure 7) support the presence of a surface oxide layer, and hence, the first assumption. The AFM images shown in Figure 1 support the second assumption, that is, that the thick 45-nm Ag underlayer and the overall 70-nm overlayer/underlayer substrate have different surface morphologies.

If the Ag underlayer is truly passivated by an oxide layer and has a morphology that is determined and fixed prior to the formation of the Ag overlayer, then the two Ag surfaces could act as individual entities that give rise to separate electric fields. Under these circumstances, a mutual coupling of electromagnetic waves from the EM fields produced by both metal surfaces could give rise to the observed SERS enhancement of the analyte from the combined electric field produced by the two interfaces.

To test this hypothesis, an experiment was performed in which a 45-nm thick Ag underlayer substrate was prepared using standard vapor deposition conditions. After oxidation of the Ag in ambient conditions, an overlayer of 24-nm Au was vapor-deposited onto the surface of the Ag/Ag₂O underlayer. The final Ag/Ag₂O/Au substrate resembles the overlayer/underlayer Ag/Ag₂O/Ag substrate described in this article but with some significant differences. Au has similar lattice constants as Ag,

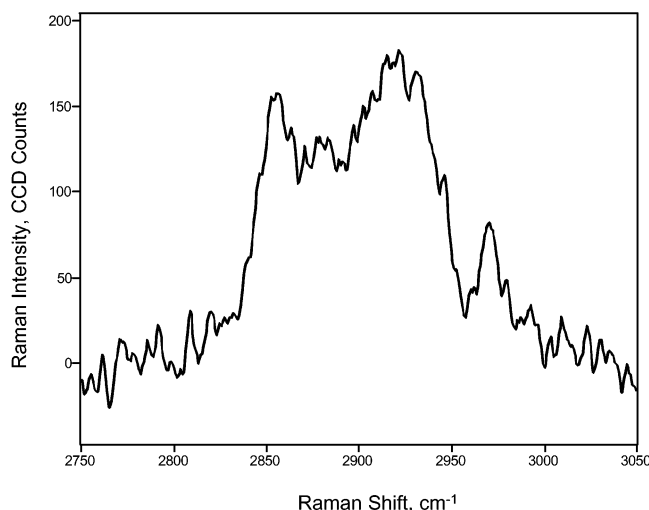


Figure 8. SERS spectrum of the $\nu(\text{C-H})$ stretching region of a 1-dodecanethiol SAM adsorbed onto a dual overlayer/underlayer substrate constructed of an underlayer of 45-nm Ag and an overlayer of 24-nm Au (Ag/Ag₂O/Au). Excitation wavelength 514.5 nm, 150 mW laser power, 60 s integration time with 10 coadds.

so the vapor deposition of an overlayer of Au should mimic the morphology of the Ag overlayer, with the exception that the Au atoms will not be affected by the surface oxide. In addition, Au is not SERS active using 514.5-nm excitation. Therefore, no electric field, and hence no SERS enhancement, should arise from the Au overlayer. Under these circumstances, any SERS enhancement that is observed must originate from the presence of the electric field of the Ag underlayer surface alone.

Alkanethiols are known to form well-ordered monolayers upon self-assembly on Au. To show that a thick Au substrate itself has no SERS activity using visible excitation, a 25-nm thick Au substrate was prepared and a 1-dodecanethiol SAM was prepared on its surface. This surface showed no SERS intensity with excitation at 514.5 nm. A 1-dodecanethiol SAM was then prepared on the Au surface of a 45-nm oxidized Ag underlayer and a 25-nm thick Au overlayer (Ag/Ag₂O/Au) and its SERS spectrum was obtained using 514.5-nm excitation. Figure 8 shows the SERS spectrum in the C-H stretching region of this SAM. The SERS intensities obtained from a SAM on the Ag/Ag₂O/Au substrate are significantly weaker than are the intensities for a 1-dodecanthiol SAM on the Ag/Ag₂O/Ag substrate (compare, e.g., Figure 8 with Figure 2A.b). Since the Au overlayer does not contribute to the observed SERS intensities, Figure 8 demonstrates that the laser excitation can penetrate into the Ag/Ag₂O underlayer and that the electric field produced from this buried surface will interact with the SAM on top of the Au overlayer. Other studies have shown that the electric field from a SERS-active metal can penetrate through a nonenhancing overlayer for studies of adsorbed molecules.^{16,23,40–42} Although it is possible to generate a SERS spectrum with a nonenhancing overlayer, the weak SERS intensities shown in Figure 8 generated by the Ag/Ag₂O underlayer also demonstrate that a combined electric field from both the Ag/Ag₂O underlayer and the Ag overlayer is necessary to generate the large SERS enhancements we observe for the Ag/Ag₂O/Ag overlayer/underlayer substrate (Figure 2).

Conclusions

A novel substrate for SERS has been developed that consists of a vapor-deposited overlayer of Ag on an underlayer of

chemisorbed Ag₂O on Ag (Ag/Ag₂O/Ag). The total thickness of this substrate is ~ 70 nm. Raman intensity increases of $\sim 400\%$ for 1-dodecanethiol SAMs are achieved using this substrate when compared to traditional thick Ag films. Relative to the bulk phase, the SERS enhancement factor calculated for this new substrate is approximately 10^4 in magnitude, which is comparable to the SERS intensity enhancements achieved using thin, vapor-deposited AgIFs. AFM results show that the outermost Ag overlayer particles have ideal shapes for SERS enhancement with morphology comparable to the thin, vapor-deposited AgIFs that have been previously shown to give maximal SERS response. XPS data showed that surface of the Ag/Ag₂O underlayer was clean and identified the source of the trace contaminants to be oxygen and carbon. Investigation of the XPS O(1s) region showed the presence of multiple forms of oxygen in the Ag/Ag₂O underlayer; the main forms were identified as dissolved bulk oxygen as well as chemisorbed oxygen.

These new dual-layer substrates are easy to produce and consist of a uniform surface that leads to more reproducible SERS intensities for the Ag/Ag₂O/Ag substrate (RSD = 0.45–5%) compared to traditional thick Ag films (RSD = 12–28%). The Raman intensity enhancements achieved on this new substrate are believed to be the result of ideal morphology of the Ag particles on the overlayer surface as well as a combined electric field effect produced from the Ag/Ag₂O underlayer and Ag overlayer surfaces.

Acknowledgment. We would like to thank Dr. Brian W. Gregory and Dr. John L. Stickney for many helpful discussions. The research presented here was supported by the U.S. Public Health Service through National Institute of Health grant GM40117 (R.A.D.).

References and Notes

- (1) Fleischmann, M.; Hendra, P. J.; McQuillan, A. J. *Chem. Phys. Lett.* **1974**, *26*, 163.
- (2) Campion, A.; Kambhampati, P. *Chem. Soc. Rev.* **1998**, *27*, 241.
- (3) Jeanmaire, D. L.; Van Duyne, R. P. *J. Electroanal. Chem.* **1977**, *84*, 1.
- (4) Albrecht, M. G.; Creighton, J. A. *J. Am. Chem. Soc.* **1977**, *99*, 5215.
- (5) Otto, A.; Mrozek, I.; Grabhorn, H.; Akermann, W. *J. Phys.: Condens. Matter* **1992**, *4*, 1143.
- (6) Cotton, T. M.; Brandt, E. S. *Surface-Enhanced Raman Scattering*. In *Physical Methods of Chemistry*; John Wiley & Sons: New York, 1992; p 633.
- (7) Ruperez, A.; Laserna, J. J. *Surface enhanced Raman spectroscopy*. In *Modern Techniques in Raman Spectroscopy*; Laserna, J. J., Ed.; John Wiley & Sons: Chichester, U.K., 1996; p 227.
- (8) Cotton, T. M. The application of surface-enhanced Raman scattering to biochemical systems. In *Spectroscopy of Surfaces*; Clark, R. J. H., Hester, R. E., Eds.; John Wiley and Sons: New York, 1988; p 91.
- (9) Moskovits, M. *Rev. Mod. Phys.* **1985**, *57*, 783.
- (10) Pemberton, J. E. Surface enhanced Raman scattering. In *Electrochemical Interfaces. Modern Techniques for In-Situ Characterization*; Abruna, H. D., Ed.; VCH Verlag Chemie: Berlin, 1991; p 195.
- (11) Weaver, M. J.; Zou, S. Vibrational spectroscopy of electrochemical interfaces. Some walls and bridges to surface science understanding. In *Spectroscopy for Surface Science*; Clark, R. J. H., Hester, R. E., Eds.; Advances in Spectroscopy, Vol. 26; John Wiley & Sons: Chichester, U.K., 1998; p 219.
- (12) Chang, R. K.; Furtak, T. E. *Surface Enhanced Raman Scattering*; Plenum: New York, 1982.
- (13) Gersten, J.; Nitzan, A. *J. Chem. Phys.* **1980**, *73*, 3023.
- (14) Metiu, H.; Das, P. *Annu. Rev. Phys. Chem.* **1984**, *35*, 507.
- (15) Gersten, J.; Nitzan, A. Electromagnetic Theory: A Spheroidal Model. In *Surface Enhanced Raman Scattering*; Furtak, T. E., Ed.; Plenum: New York, 1982; p 89.
- (16) Murray, C. A. *J. Electron Spectrosc. Relat. Phenom.* **1983**, *29*, 371.
- (17) Murray, C. A.; Allara, D. L.; Rhinewine, M. *Phys. Rev. Lett.* **1981**, *46*, 57.
- (18) Murray, C. A.; Allara, D. L. *J. Chem. Phys.* **1982**, *76*, 1290.

- (19) Murray, C. A.; Allara, D. L.; Hebard, A. F.; Padden, J. F., Jr. *Surf. Sci.* **1982**, *119*, 449.
- (20) Cotton, T. M.; Uphaus, R. A.; Möbius, D. *J. Phys. Chem.* **1986**, *90*, 6071.
- (21) Mrozek, I.; Otto, A. *Europhys. Lett.* **1990**, *11*, 243.
- (22) Compagnini, G.; Galati, C.; Pignataro, S. *Phys. Chem. Chem. Phys.* **1999**, *1*, 2351.
- (23) Kennedy, B. J.; Spaeth, S.; Dickey, M.; Carron, K. T. *J. Phys. Chem. B* **1999**, *103*, 3640.
- (24) Schlegel, V. L.; Cotton, T. M. *Anal. Chem.* **1991**, *63*, 241.
- (25) Bryant, M. A.; Pemberton, J. E. *J. Am. Chem. Soc.* **1991**, *113*, 3629.
- (26) Roy, D.; Furtak, T. E. *Chem. Phys. Lett.* **1986**, *124*, 299.
- (27) Neddersen, J.; Chumanov, G.; Cotton, T. M. *Appl. Spectrosc.* **1993**, *47*, 1959.
- (28) Norrod, K. L.; Sudnik, L. M.; Rousell, D.; Rowlen, K. L. *Appl. Spectrosc.* **1997**, *51*, 994.
- (29) Van Duyne, R. P.; Hulteen, J. C.; Treichel, D. A. *J. Chem. Phys.* **1993**, *99*, 2101.
- (30) Aktsipetrov, O. A.; Nikulin, A. A.; Panov, V. I.; Vasil'ev, S. I.; Petukhov, A. V. *Solid State Commun.* **1990**, *76*, 55.
- (31) Goss, C. A.; Charych, D. H.; Majda, M. *Anal. Chem.* **1991**, *63*, 85.
- (32) Moulder, J. F.; Stickle, W. F.; Sobol, P. E.; Bomben, K. D. *Handbook of X-ray Photoelectron Spectroscopy: A Reference Book of Standard Spectra for Identification and Interpretation of XPS Data*; Perkin-Elmer Corp.: Eden Prairie, MN, 1992.
- (33) Leverette, C. L.; Dluhy, R. A. *Langmuir* **2000**, *16*, 3977.
- (34) Hill, W.; Rogalla, D. *Anal. Chem.* **1992**, *64*, 2575.
- (35) Swalen, J. D.; Allara, D. L.; Andrade, J. D.; Chandross, E. A.; Garoff, S.; Israelachvili, J.; McCarthy, T. J.; Murray, R.; Pease, R. F.; Rabolt, J. F.; Wynne, K. J.; Yu, H. *Langmuir* **1987**, *3*, 932.
- (36) Weiping, C.; Ming, T.; Lide, Z. *J. Phys. Condens. Matter* **1997**, *9*, 1995.
- (37) Bao, X.; Muhler, M.; Schedel-Niedrig, T.; Schlögl, R. *Phys. Rev. B* **1996**, *54*, 2249.
- (38) Boronin, A. I.; Koscheev, S. V.; Zhidomirov, G. M. *J. Electron Spectrosc. Relat. Phenom.* **1998**, *96*, 43.
- (39) Yu, H. Z.; Zhang, J.; Zhong, H. L.; Liu, Z.-P. *Langmuir* **1999**, *15*, 16.
- (40) Lacy, W. B.; Williams, J. M.; Wenzler, L. A.; Beebe, T. P., Jr.; Harris, J. M. *Anal. Chem.* **1996**, *68*, 1003.
- (41) Walls, D. J.; Bohn, P. W. *J. Phys. Chem.* **1989**, *93*, 2976.
- (42) Wasileski, S. A.; Zou, S.; Weaver, M. J. *Appl. Spectrosc.* **2000**, *54*, 761.